ICE CLOUD RETRIEVAL IN THE MARTIAN ATMOSPHERE USING SPICAM/UV.

Y. Willame, A.C. Vandaele, *IASB-BIRA, Brussels, Belgium (yannick.willame@aeronomie.be)*, **B. Gondet,** *IAS, Paris, France*, **F. Montmessin,** *LATMOS, Paris, France*.

Introduction

The SPICAM instrument on board Mars-Express (MEX) provides valuable data to investigate the Martian atmosphere since 2004. The UV channel, a spectrometer operating in the spectral interval between 110-320 nm, has been in activity during 11 years. The nadir viewing mode records the solar radiation that has been scattered and reflected by the planet and its atmosphere. From these measurements, we can deduce the amounts of several atmospheric species such as dust, ice clouds [Mateshvili *et al.*, 2007,2009] and ozone [Perrier *et al.*, 2006] but also the surface albedo.

We have developed an improved retrieval algorithm using a more recent and up-to-date parametrisation of the atmosphere and surface characteristics than in previous SPICAM works. The purpose is to deduce simultaneously the following parameters: the ozone column, the dust optical depth (OD), the cloud OD and the surface reflectance. In order to keep independent parameters, the retrieval was limited to 3 parameters. The choice of the non retrieved parameter is made between the cloud OD and the surface albedo for each measurement and depends on the cloud presence. We have therefore developed a cloud detection algorithm from which the results have been compared to those of MEX/OMEGA.

More than 4 Martian years (MY27-30) of SPICAM UV data have been analysed with our retrieval method to produce climatologies of the 4 studied parameters. We will present the results obtained for clouds: the principle of the cloud detection algorithm and the climatology of the retrieved cloud OD obtained using our retrieval method.

Cloud detection method

Clouds appear very bright in the UV compared to the "dark" regolith surface and result in the measurements by an increase of the recorded signal. More precisely, the increase of signal is proportionally more important at longer wavelengths than at shorter wavelengths in the interval considered (220-290 nm). The principle of detection is thus based on the combination of two characteristics: a relatively large increase of the averaged signal (S_{av}) and an increase of longer/shorter wavelength ratio (or colour ratio: R_{rb}). This combination allows to differentiate from the effects due to dust, ozone and Rayleigh scattering. However, the surface

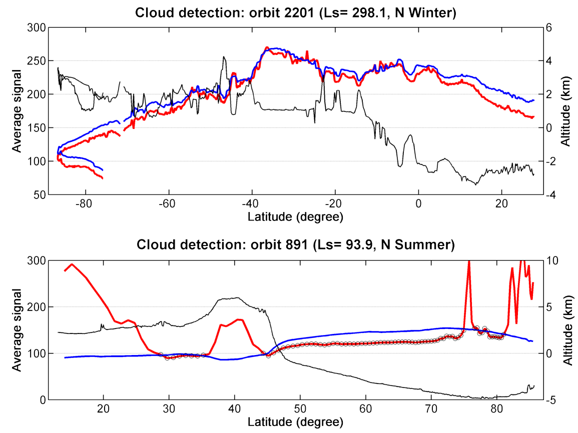

Figure 1: Example of cloud detection for orbit 2201 and 891. The averaged signal S_{av} is represented in red and its associated estimation Est_{av} in blue. The evolution of the surface elevation is given in thin black line (the altitude-scale is given on the right-side of each plot). For orbit 2201, no cloud is present and all the measurements were selected as CIF references. For orbit 891, the measurements selected as CIF references are marked with black circles. Three possible cloud detections were performed: two clear detections above regolith region ([14°N-28°N] and [36°N-44°N], both confirmed by OMEGA); and a detection in an "uncertain" area ([75°N-77°N], identified as H_2O ice surface by OMEGA). No detection was performed above 81°N as the presence of ice was predicted.

reflection also shows such a combination, but as the regolith is strongly absorbing, it induces only limited signal variations and can be differentiated by choosing an adapted (large enough) threshold. On the contrary, ice surface is very bright and can not be differentiated by such a threshold. Area covered by ice, based on the MCD (Mars Climate Database) v5.0 predictions, were therefore excluded in the cloud detection. An "uncertain" area of about 10° latitude is also delimited at the edge of the ice caps, and in which the detections must be considered with caution as it could have been induced by the unpredicted presence of ice.

Each orbit is analysed separately. We simulate an averaged estimate signal Est_{av}, analogous to S_{av}, using the *a priori* values (atmospheric parameters from MCD and regolith surface parameters from [Wolff *et* *al.*, 2014]). The idea being that $\text{Est}_{av}(i_m)$ should follow the $\text{S}_{av}(i_m)$ variations relatively closely for all i_m measurements wherein no cloud nor ice are present, while for the measurements affected by the presence of clouds or ice, S_{av} would increase relatively to Est_{av}.

Figure 1 shows the examples of orbit 2201 and 891. Est_{av} is used to select the cloud- and ice-free (CIF) reference measurements (i.e. all the measurements for which S_{av} remains close or below to Est_{av}). These CIF measurements are then used to build a CIF averaged signal $\text{S}_{av}^{\text{ref}}$ (resp. a CIF colour ratio $\text{R}_{rb}^{\text{ref}}$) to which S_{av} (resp. R_{rb}) is then compared in order to determine if the cloud detection threshold t_{av} (resp. t_{rb}) is exceeded. A cloud is detected when both conditions are verified:

$$\begin{cases} \text{S}_{av}(i_m) > (1+\text{t}_{av})\ \text{S}_{av}^{\text{ref}}(i_m) \\ \text{R}_{rb}(i_m) > (1+\text{t}_{rb})\ \text{R}_{rb}^{\text{ref}}(i_m) \end{cases}$$

where $\text{S}_{av}^{\text{ref}}$ (resp. $\text{R}_{rb}^{\text{ref}}$) is obtained from S_{av} (resp. R_{rb}) using a weighted average on the nearest CIF measurements (the weight depends on the spatial proximity and surface elevation).

Comparison with OMEGA

We have performed a comparison of our detection results with those obtained by OMEGA, also on board MEX. Their method uses the 3.1 μm water ice absorption band, considering the slope on the edge of the band between 3.4-3.52μm to derive the "cloud index" [Langevin *et al.*, 2007]. OMEGA can make the difference between ice cloud and ice surface (and also between H_2O and CO_2 ice) which is useful to validate our detection method. The comparison was performed on simultaneous observations of both instruments. This is important for cloud detection as clouds can appear and disappear relatively quickly following the temperature variations.

A detailed comparison was performed with the cloud index maps derived in Madeleine *et al.*, 2012 for the Tharsis region and its vicinity, revealing a very good agreement (in terms of location and extension) for clouds with moderate-to-large OD (retrieved afterwards). For clouds with lower OD, at which the OMEGA method is estimated to reach its detection limit, OMEGA performs still some faint detections that are usually seen by SPICAM (with some additional detections with SPICAM).

Comparisons were also performed in the vicinity of the polar caps where our detection must be considered with caution due to the potential presence of unpredicted ice on the surface. The comparison with OMEGA's results shows a reasonable agreement between the two methods: the detections (of ice or clouds) correspond, however their spatial extension is not always in perfect agreement.

The comparison with OMEGA results tends to validate our detection algorithm.

Cloud climatology

The cloud climatology presented here has been obtained by analysing more than 4 Martian years of SPICAM/UV measurements with the detection algorithm combined with the retrieval algorithm.

Figure 2 shows the seasonal evolution of the cloudiness on Mars, averaged latitudinally and on the 4 MYs. It illustrates the different cloud features that appear on Mars throughout the year. The two main features are: the aphelion cloud belt (ACB) that occurs every year at low latitudes during the aphelion season and the polar hoods that occur above the polar regions of the winter hemisphere.

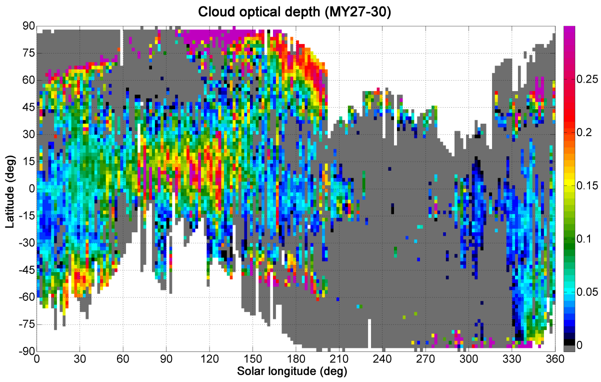

Figure 2: Seasonal evolution of the zonally averaged cloud opacity. The values are averaged on the four Martian years of the dataset (from MY: 26.9 to 31.0) using a $2° \times 2°$ grid. The grey background represents the measurement coverage and the colour scale ranging from black to purple indicates the retrieved cloud opacity.

The spatial and seasonal evolution of the ACB was analysed, showing its different stages as visible in figure 2: the formation starts around $L_s = 20 - 30°$, it shows a maximum extension and intensity between $L_s = 80°$ and $L_s = 140°$ and quickly disappears after $L_s = 140°$. The spatial extension for the ACB maximum activity, when clouds form a belt all around the equator, is shown in figure 3. The highest opacities are observed above the Tharsis region, Lunae Planum and over in the vicinity of Olympus and Elysium volcanoes. These seasonal and spatial distributions are in agreement with the results of Smith *et al.*, 2004 using MGS/TES.

The largest values of cloud OD are often found above the high volcanoes. These orographic clouds form because of adiabatic cooling that occurs with upslope winds arising on these volcanoes. This process makes these locations particularly favourable for cloud formation. As shown in figure 4, we have analysed the seasonal evolution of the cloudiness above the six tallest volcanoes and compared it to the results of Benson *et al.*, 2006 obtained using MGS/MOC: the periods

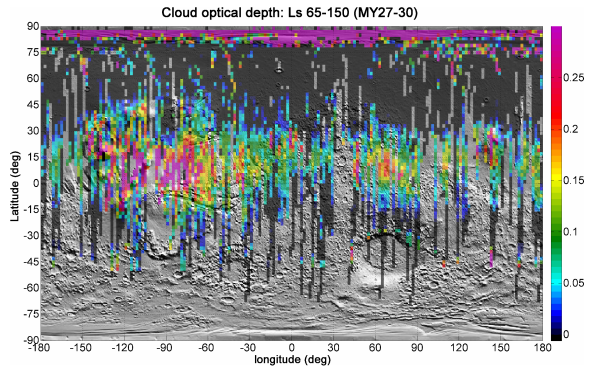

Figure 3: Spatial distribution of the cloud optical depth for the period going from L_s = 65-150°. The map is averaged on a 2° × 2° grid and was obtained for the complete dataset (MY: 26.9 to 31.0). Darkened pixels indicates the measurement coverage and the colour scale ranging from black to purple corresponds the retrieved cloud opacity.

where clouds are observed with SPICAM and MOC shows generally a good general agreement indicating a year-to-year repeatability (as the measurements from both instruments do not overlap in time). A correlation between the spatial extension derived by MOC and the OD of clouds obtained from SPICAM is sometimes observed.

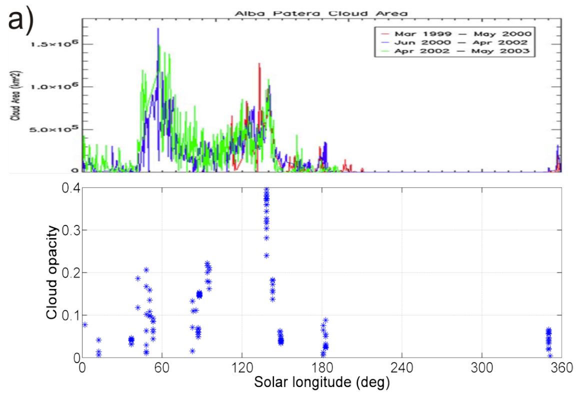

Figure 4: Visual comparisons between the retrieved cloud opacity from this work (blue symbols, bottom panel) and the total cloud area (km^2, upper panel with MY 24, 25 and 26 represented respectively by red, blue and green lines) obtained by Benson *et al.*, 2006. The seasonal evolution is shown for Alba Mons.

The edge of the polar hoods were observed at certain periods as visible in figure 2. For example, the northern polar hood (NPH) was clearly observed with SPICAM between L_s = 150-200°. We observe that it starts to form around L_s = 150° and expands progressively equatorward and grows in thickness until L_s = 200°. The spatial distribution for this period is shown in figure 5 indicating that all longitudes are covered by the polar hood. The NPH reaches generally latitudes down to 45°N but deviations are visible : the hood extends a little further south in the longitude band going from 170°W to 30°W. This seasonal and spatial behaviours are in agreement with the NPH results of Benson *et al.*, 2011 obtained from MRO/MCS. The edges of the NPH was also observed between L_s = 220-260° and between L_s = 330-20° (see figure 2). The results for southern polar hood were also considered, and were compared those obtained in Benson *et al.*, 2010 using MRO/MCS and shows also generally a reasonable agreement concerning the seasonal and spatial distributions.

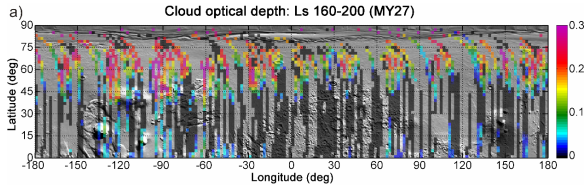

Figure 5: Optical depth (colour scale) of the north polar hood (NPH) for the period between L_s = 160-200° of MY27. The map is limited to the northern hemisphere.

Summary

We have shown that the cloud detection method we have developed for our retrieval algorithm using SPICAM/UV is working properly, giving results in agreement with the detection results obtained from simultaneous but independent OMEGA measurements.

The derived 4 MY cloud climatology offers a good representation of the different cloud features (ACB, polar hoods, orographic clouds) observed outside of the winter polar regions. It allows the study of their seasonal and spatial distributions. Our results generally concord with other work results derived from other instruments (MEX/OMEGA, MGS/TES, MGS/MOC, MRO/MCS).

References

Benson *et al.*, 2006, Icarus, 184, doi:10.1016/j.icarus.2006.03.014

Benson *et al.*, 2010, J. Geophys. Res., 115, doi:10.1029/2009JE003554

Benson *et al.*, 2011, J. Geophys. Res., 116, doi:10.1029/2010JE003693

Langevin *et al.*, 2007, J. Geophys. Res., 112, doi:10.1029/2006JE002841

Madeleine *et al.*, 2012, J. Geophys. Res., 117, doi:10.1029/2011JE003940

Mateshvili *et al.*, 2007, J. Geophys. Res., 112, doi:10.1029/2006JE002827

Mateshvili *et al.*, 2009, Planet Space Sci, 57, doi:10.1016/j.pss.2008.10.007

Perrier *et al.*, 2006, J. Geophys. Res., 111, doi:10.1029/2006JE002681

Smith *et al.*, 2004, Icarus, 167, doi:10.1016/j.icarus.2003.09.010

Wolff *et al.*, 2014, MAMO 2014